**CHAPTER 7**

# SYNTHESIS AND CHARACTERIZATION OF COMPOSITES

# $BaTi_{0.85}Sn_{0.15}O_3$ – FLY ASH

## 7.1 INTRODUCTION

Coal is the largest source of energy for the generation of electricity worldwide accounting for approximately 36% of the world's electricity production. A huge amount of fly ash is produced during coal burning posing an increasing concern in its recycling. The production of fly ash by these thermal power plants may cross over 100 million tons in this decade [232, 233]. The availability of the minerals in coals is classified into one of four groups: alumino silicates (including clay), carbonates, sulphides and silica (quartz) [234]. During combustion some minerals such as clay may be altered thermally, while other minerals, such as quartz may remain unaltered .The thermally treated coal impurities, along with small amount of unburned coal, makeup the fly ash. The composition of the coal impurities is not fixed. Thus the composition of resulting fly ash also varies. The major constituents of fly-ash are α-quartz ($SiO_2$), mullite ($3Al_2O_3.2SiO_2$), hematite ($Fe_2O_3$), magnetite ($Fe_3O_4$), lime (CaO) and gypsum ($CaSO_4.2H_2O$) [235].

Fly ash a waste material has various useful compounds and elements. It is reported that flyash generally contains elements like Cu, Pb, Cd, Ag, Mo, Fe, Ti, Na, Mn, S, P Zn and Cl in different concentrations which depends upon the variety of coal used.

Many investigators have studied the use of fly ash with cement, organic and inorganic materials. In cement production fly ash is an additive material. The granulometry and fineness of fly ashes have effect of mortar compressive strength [236]. The development of fly ash-based

inorganic polymeric materials for construction of building purposes [237]. The incorporation of FA into the polymeric network introduces uniform porosity and is expected to be advantageous for gas sensing and bio sensing applications [238].

The solid solution of ferroelectric $BaTiO_3$ and non-ferroelectric BaSnO3 makes useful for various applications like sensor, thermally stable capacitor, microwave dielectric etc. The relaxor properties of solid solution BTS have been well stabilized for doping concentration of 15 % Sn in the lattice of $BaTiO_3$ which makes this system multifunctional materials than their host. Various studies on the composite of two such as ceramics including $BaTiO_3$, $BiFeO_3$, PZT, $BaSnO_3$ etc. with Fly-ash have been carried out [239,240] to explore application in phase shifter, thermally stable capacitor, mechanically strength material etc. No studies have been made on the composite of relaxor $BaTi_{0.85}Sn_{0.15}O_3$ (BTS) with fly-ash. To the best of our knowledge this will be the probably first report. In order to convert waste material fly ash into useful material we have tried to synthesized composites of $BaTi_{0.85}Sn_{0.15}O_3$ with fly ash. We have kept processing parameters exactly same as were for the synthesis of composites discussed in the previous chapters.

## 7.2 RESULTS AND DISCUSSION

Synthesis of powder of $BaTi_{0.85}Sn_{0.15}O_3$ (abbreviated as BTS) has already been described in details in chapter 3. Fly ash used in this work was collected from the Koradi Thermal power plant, Nagpur, Maharashtra. Composites with general formula (1-x) $BaTi_{0.85}Sn_{0.15}O_3$ (BTS) + (x) Fly Ash (FA) (x=5 %, 10 %, 15 % and 20%) were prepared by mixing calculated amounts of powder of BTS and Fly Ash. These composites have been referred throughout this chapter by abbreviated name BTS-FA5 (for $x$ = 5%), BTS-FA10 (for $x$ = 10%), BTS-FA15 (for $x$ = 15%) and BTS-FA20 (for x=20%).

### 7.2.1 Thermal Analysis

Thermal analysis (TG and DSC) of the fly ash powder and mixture for one of the composite BTS-FA20 obtained after milling was carried out using simultaneous TG-DSC (Metller Toledo) thermal analyzer in the temperature range 30–1000 °C with a heating rate of 10 °C/min in nitrogen atmosphere. TG-DSC curves of the Fly Ash and mixture for composite BTS-FA20 are shown in Figure 7.1 and 7.2 respectively. TG curve of fly ash has shown only 0.20 % weight loss in the temperature range 30 - 1000 $^{o}$C. This small amount of weight loss may be due to small content of the carbon present in the fly ash. In the DSC curve a weak endothermic peak around 970$^{o}$C is observed. As it is mentioned earlier that fly ash contains compounds; quartz ($SiO_2$), aluminate ($Al_2O_3$), hematite ($Fe_2O_3$), magnetite ($Fe_3O_4$), lime (CaO) and gypsum ($CaSO_4.2H_2O$) etc. At higher temperature these compounds may react with each other and form new phase. It is reported in the literature that $Al_2O_3$ and $SiO_2$ present in the fly ash react at higher temperature and form mullite [241]. Thus observed weak endothermic peak may be attributed to the formation of mullite phase due to reaction among the constituents of fly ash.

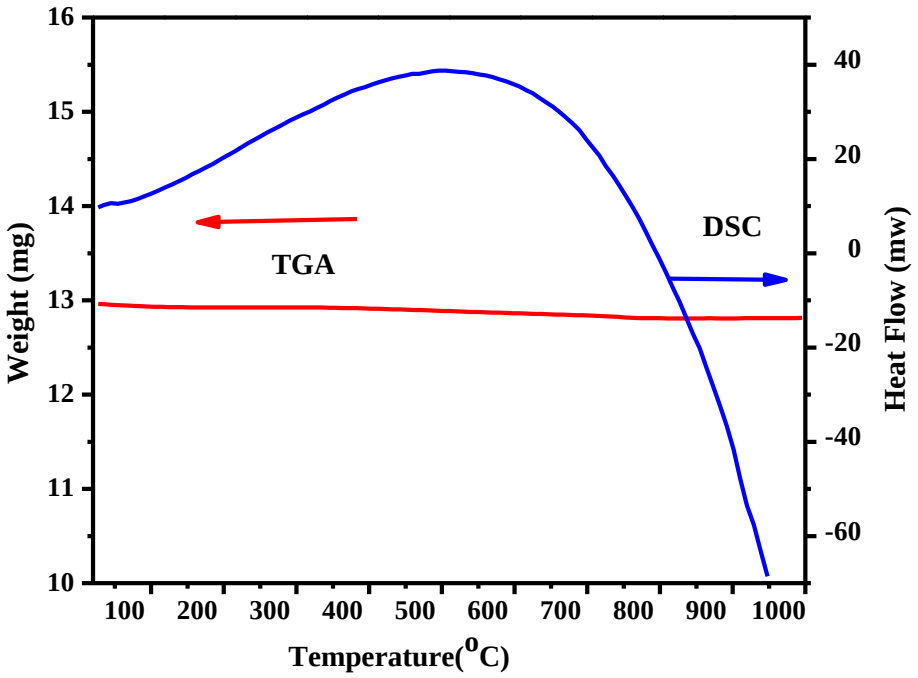


**Figure 7.1** TGA-DSC curve of Fly ash (FA)

Figure 7.2 shows TG-DSC curves of the mixture of BTS and 20 wt % fly ash obtained after ball milling for 8 h using a planetary ball mill. TG curve shows total weight loss approximately 1.11% in two steps. The first step weight loss (approximately 0.25 %) in temperature range 30-160$^{o}$C may be due to evaporation of remaining amount of acetone (used for mixing) or evaporation of water molecules adsorbed on the surface of BTS particles. The second step weight loss (approximately 0.86 %) in the temperature range 500-600$^{o}$C is assigned to the burning of carbon containing compound present in the sample. There is no distinct peak in the DSC curve of the mixture which rules out reaction between BTS and Fly ash up to 1000$^{o}$C.

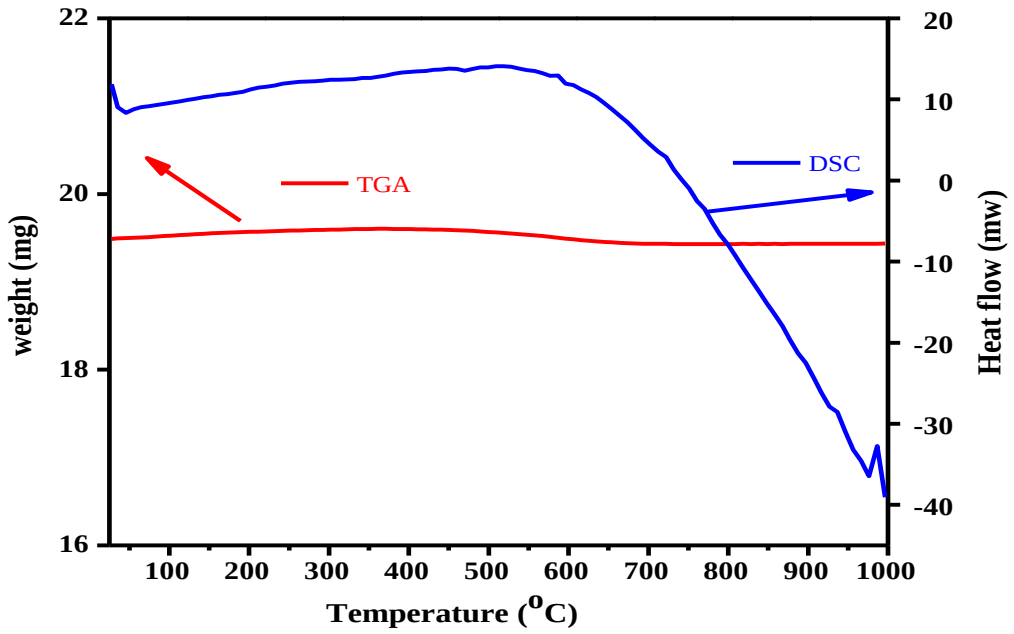


**Figure 7.2** TGA-DSC curve of mixture of composite BTS+FA20

### 7.2.2 Phase Analysis

The x-ray diffraction patterns obtained of (BTS), fly ash (FA) and their composites BTS-FA5, BTS-FA10, BTS-FA15 and BTS-FA20 are shown in Figure 7.3. The observed peaks in the XRD patterns of BTS are indexed with the help of JCPDS file (No. 31-0174) reported in the literature for cubic phase of $BaTiO_3$. In the XRD pattern of fly ash (FA) few sharp peaks are present. These peaks belong to crystalline phase of quartz and mullite present in the fly ash [242, 243]. The XRD pattern of all the composites revealed presence of peaks of both the constituents BTS and Fly ash (FA). Beside peaks of the constituents BTS and FA, a new peak at 29.64 is also present in the XRD pattern of the composites. Based on the literature new peak is assigned to a new phase of mullite. Moreover, from the result of TGA DSC of BTS-CNT20, the presence of an endothermic peak around 920$^{o}$C this is attributed to the formation of a new phase of mullite. With increasing the content of Fly-ash (which have also some other phase of CaO around 1.1%)

combined with mullite and increase their intensity for composite BTS-CNT10, BTS-CNT15 and BTS-CNT20 respectively. This peak is well matched with the earlier report, reported by the authors in literature [244, 245].

The average crystallite size (D) of the sintered powders of BTS, BTS-FA5, BTS-FA10, BTS-FA15, BTS-FA20 and FA was calculated from the X-ray line broadening of the (110) peak and for FA sample (311) peak using Scherer's formula (equation 2.2). The value of crystallite size of all the samples are given in Table 7.1

**Table 7.1** Composite, crystallite size, strain, physical parameter (Dielectric constant, dissipation factor and conductivity) at room temperature

| **Composites** | **Crystallite size(nm)** | **Volume fraction** | | **Physical parameter at Room temperature** | | | |
|---|---|---|---|---|---|---|---|
| | | **BTS** | **FA** | **$\varepsilon_r$ (Dielectric constant)** | **$\varepsilon_r$ (Dielectric constant) using eqn (7.1)** | **D (Dissipation factor)** | **σ (ac-conductivity)** |
| BTS | 39.58 | 1 | 0 | 2684.42 | 2684.42 | 0.17513 | $3.34 \times 10^{-5}$ |
| BTS-FA5 | 35.00 | 0.82 | 0.18 | 450.82 | 895.36 | 0.25530 | $1.45 \times 10^{-8}$ |
| BTS-FA10 | 34.34 | 0.68 | 0.32 | 162.94 | 387.25 | 0.92540 | $1.78 \times 10^{-8}$ |
| BTS-FA15 | 34.98 | 0.57 | 0.43 | 92.15 | 200.12 | 1.6832 | $1.98 \times 10^{-8}$ |
| BTS-FA20 | 35.73 | 0.48 | 0.52 | 19.40 | 116.95 | 1.9708 | $2.48 \times 10^{-8}$ |
| FA | 42.30 | 0 | 1 | 6.55 | 6.55 | 4.5490 | $5.26 \times 10^{-8}$ |

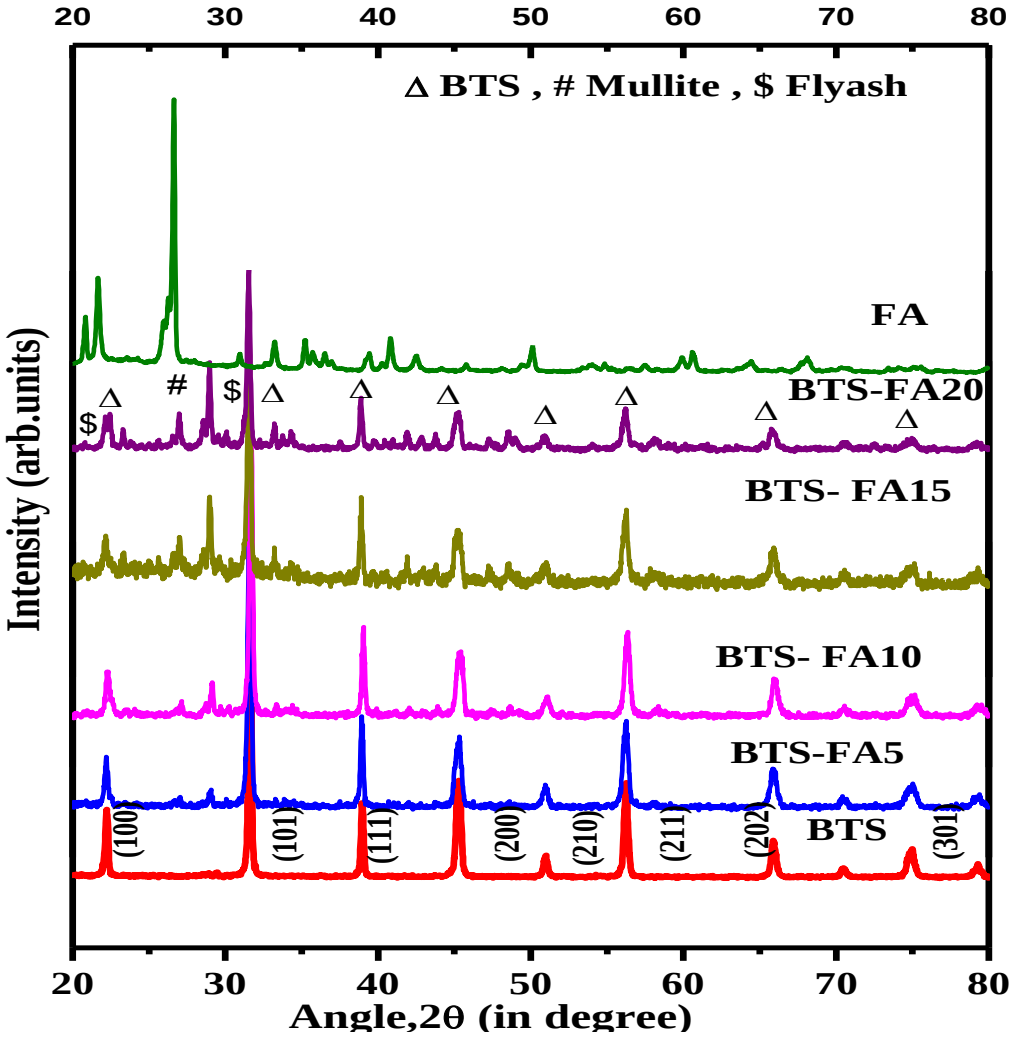


**Figure 7.3** X- ray diffraction pattern of composites BTS-FA

### 7.2.3 Fourier Transform-Infrared (FTIR) Analysis

Figure 7.4 shows the Fourier transform infrared (FTIR) spectrum in transmittance mode for three representative samples BTS, FA and BTS-FA20. From the literature, it is noted down that in the FTIR spectrum of $BaTiO_3$ and $BaSnO_3$ strong peak around 540 $cm^{-1}$and 640 $cm^{-1}$, respectively appears which is assigned to $TiO_6$ and $SnO_6$ stretching vibration that connected to the barium ion [246-249]. The position of the strongest peak of sample BTS5 is 553 $cm^{-1}$ which is due to stretching vibration of $TiO_6$ . In the FTIR spectrum of FA three bands at 440, 574 and

777 $cm^{-1}$ are present which are assigned to the bending vibrations of Si-O-Si, symmetry stretching vibrations of Si-O-Si/Al-O-Si and $AlO_4$ vibrations, respectively [250]. In the FTIR spectrum of the composite BTS-FA20 characteristics bands of both BTS and FA are present. In addition to the characteristic bands of BTS and FA a few extra bands also appeared which are identified with the help of literature. A very weak intensity peak at 2340 $cm^{-1}$ is present in the FTIR spectrum of all the samples. This peak is due to presence of $CO_2$ gas in the sample chamber [251].

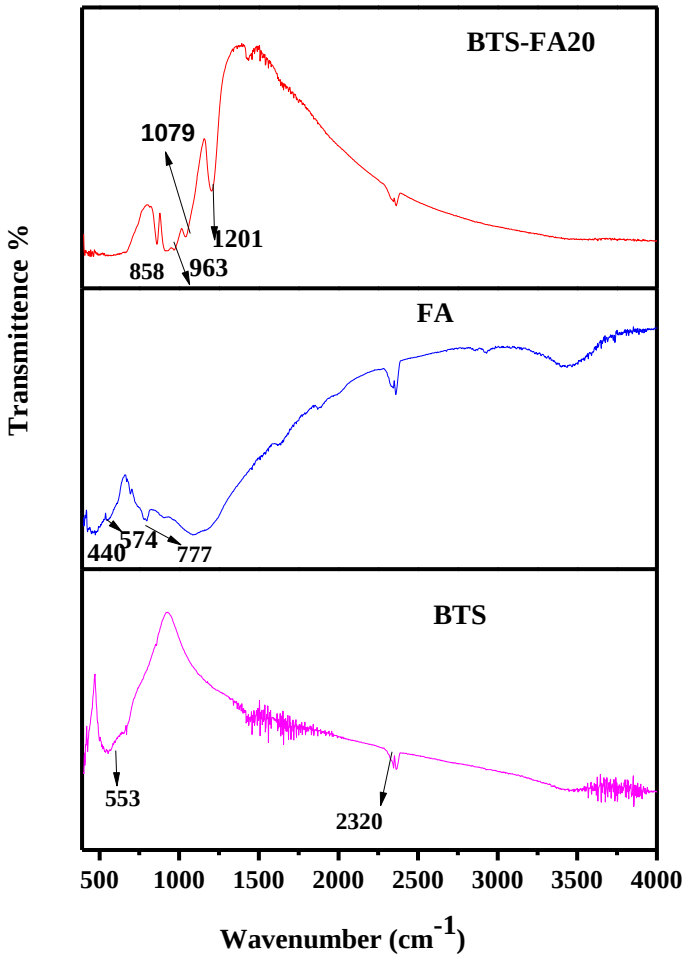


**Figure 7.4** Fourier transform infra-red spectroscopy (FTIR) of sintered samples

### 7.2.4 Scanning Electron Micrographs (SEM)

Figure 7.5 shows the scanning electron micrographs (SEM) of the fractured surfaces of BTS, FA and BTS-FA composites. SEM image of BTS shows spherical shape of grains and narrow distribution in the grain size. Scanning electron micrograph of fly ash shows the general features fly ash. As it can be seen in the figure, the fly ash is mainly constituted by compact or hollowed spheres but with a regular smooth texture. Also, some quartz particles, residue of un-burnt coal or some vitreous unshaped fragments could be seen. Microgrph of composites shows few grains of larger size as compared to other grains. Homogeneous distribution of fly ash in the matrix of BTS has taken place. The average grain size of the samples was determined using software **'ImageJ'** by obtaining the Gaussian distribution function plot for the determination of the average value of grain size for all composites as shown in Figure 7.6**.** The average **g**rain size is (0.6-1.0) μm for samples BTS-FA5, BTS-FA10, BTS-FA15and BTS-FA20, respectively. This variation in the average grain size reflects that fly-ash has been uniformly distributed on the grains of BTS, which behaves like grain growth inhibitor. Morphology of the composites particles is spherical with small grain size distribution [252]. The micrograph of composites samples (BTS-FA5, BTS-FA10, BTS-FA15and BTS-FA20) shows few grains of larger sizes as compared to other grains. Since it is observed that the grain size of fly ash is approximately 3 μm but the average grain size for composites was lying approximate in between (0.6-1.0) μm due to some agglomeration of fly ash over the BTS.

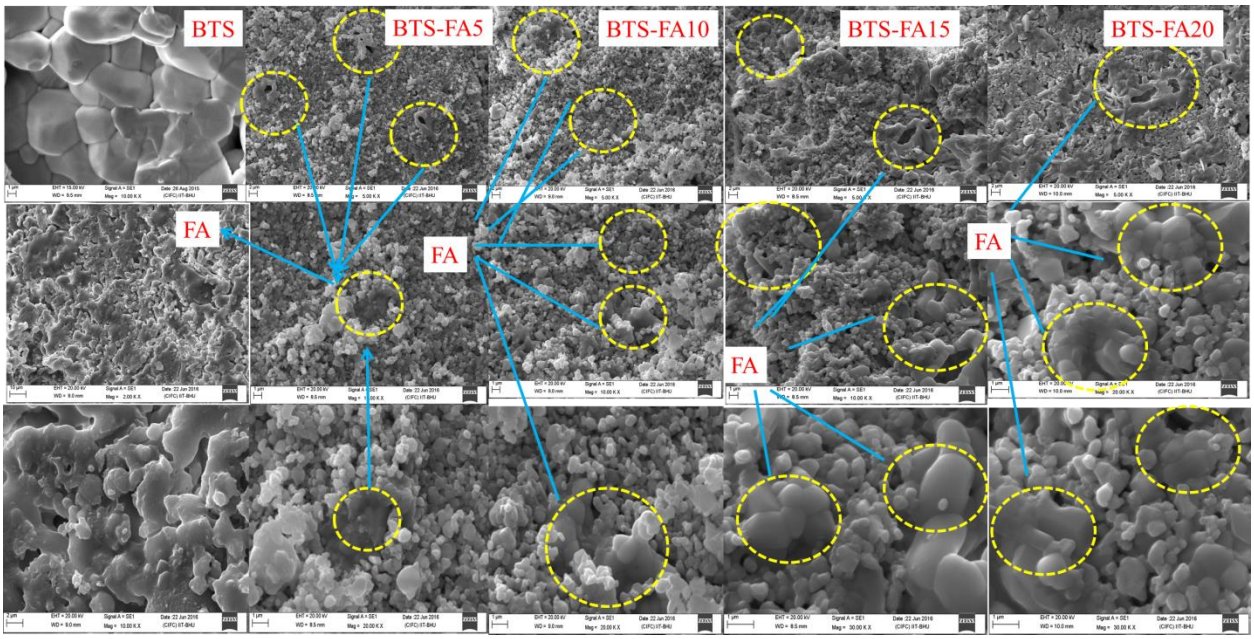


**Figure 7.5** Scanning electron micrographs of fractured surface of sintered samples

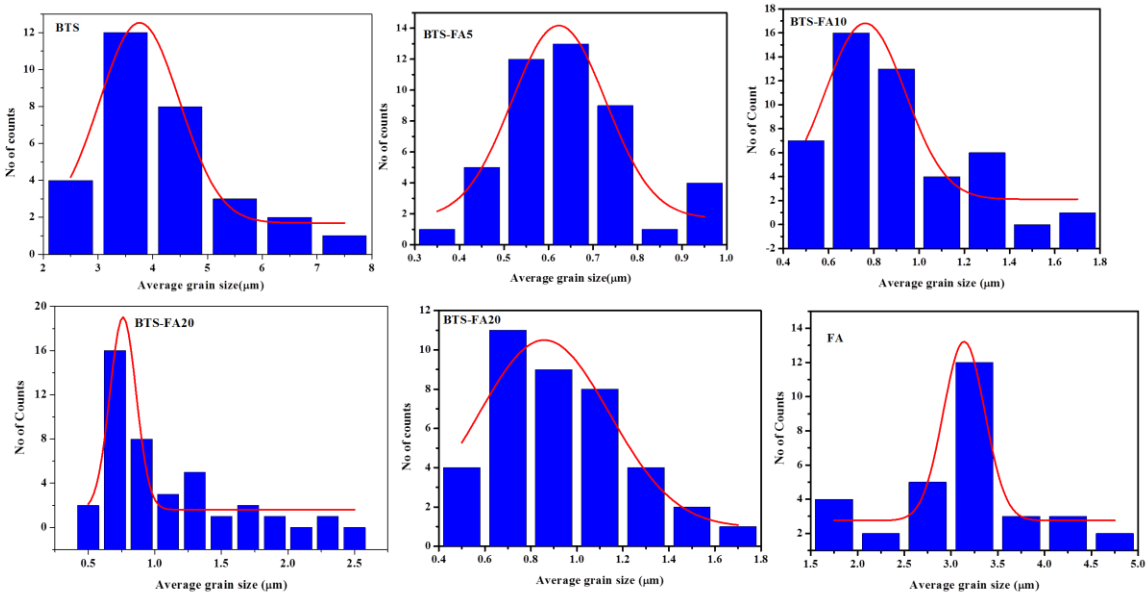


**Figure 7.6** Gaussian distribution function plot for determination of grain size of BTS and BTS-FA composites.

### 7.2.5 Energy-Dispersive X-ray (EDX) Analysis

To check the compositional homogeneity and elements present in the synthesized samples, the compositional variation (regarding concentration profile of the elements) has been probed by recording EDXA spectra of different points randomly selected in various spherical grain cores and grain boundaries. Typical EDXA spectra of the samples are shown in Figure 7.7 . It is noted that only peaks corresponding to elements Ba, Ti, Sn and O are present in the EDXA spectra of the sample BTS. In the EDXA spectrum of fly ash (FA) elements Si, Al, and Fe are present. In the EDXA spectra of composites elements Ba, Sn, Ti, O, Al, Si, Fe are present. The atomic % and weight % of these elements for all the samples are given in Table 7.2.

**Table 7.2** Compositional analysis of sintered samples

| BTS | | | FLY ASH (FA) | | | BTS-FA5 | | | BTS-FA10 | | | BTS-FA15 | | |
|---|---|---|---|---|---|---|---|---|---|---|---|---|---|---|
| **Element** | **Weight %** | **Atom %** | **Element** | **Weight%** | **Atom%** | **Element** | **Weight %** | **Atom %** | **Element** | **Weight%** | **Atom %** | **Element** | **Weight %** | **Atom %** |
| BaL | 63.19 | 24.31 | Al K | 16.06 | 12.08 | Ba L | 59.05 | 21.28 | Ba L | 58.25 | 20.09 | Ba L | 57.62 | 19.74 |
| TiK | 15.81 | 17.44 | Ti k | - | - | Ti K | 20.90 | 21.60 | Ti K | 15.86 | 15.52 | Ti | 17.36 | 17.05 |
| OK | 17.11 | 56.51 | OK | 51.80 | 65.71 | O K | 17.97 | 55.59 | OK | 19.35 | 56.71 | O K | 19.04 | 56.02 |
| SnL | 3.89 | 1.73 | Si K | 29.00 | 20.96 | Sn L | 1.47 | 0.61 | Sn L | 1.78 | 0.70 | Sn L | 2.25 | 0.89 |
| Al k | - | - | Al K | 0.77 | 0.39 | Al K | 0.41 | 0.75 | Al K | 0.41 | 0.71 | Al k | 0.71 | 1.24 |
| Si k | - | -- | Fe K | 2.36 | 0.86 | Fe | 0.20 | 0.18 | Si K | 3.74 | 6.25 | Si k | 3.01 | 5.05 |
| Total | 100 | | Total | 100 | | Total | 100 | | Total | 100 | | Total | 100 | |

| BTS-FA20 | | |
|---|---|---|
| **Element** | **Weight %** | **Atom %** |
| Ba L | 51.48 | 15.91 |
| Ti K | 17.99 | 15.54 |
| O K | 22.88 | 60.71 |
| Sn L | 3.47 | 1.24 |
| Al k | 1.17 | 1.66 |
| Si k | 3.00 | 4.54 |
| Total | 100 | |

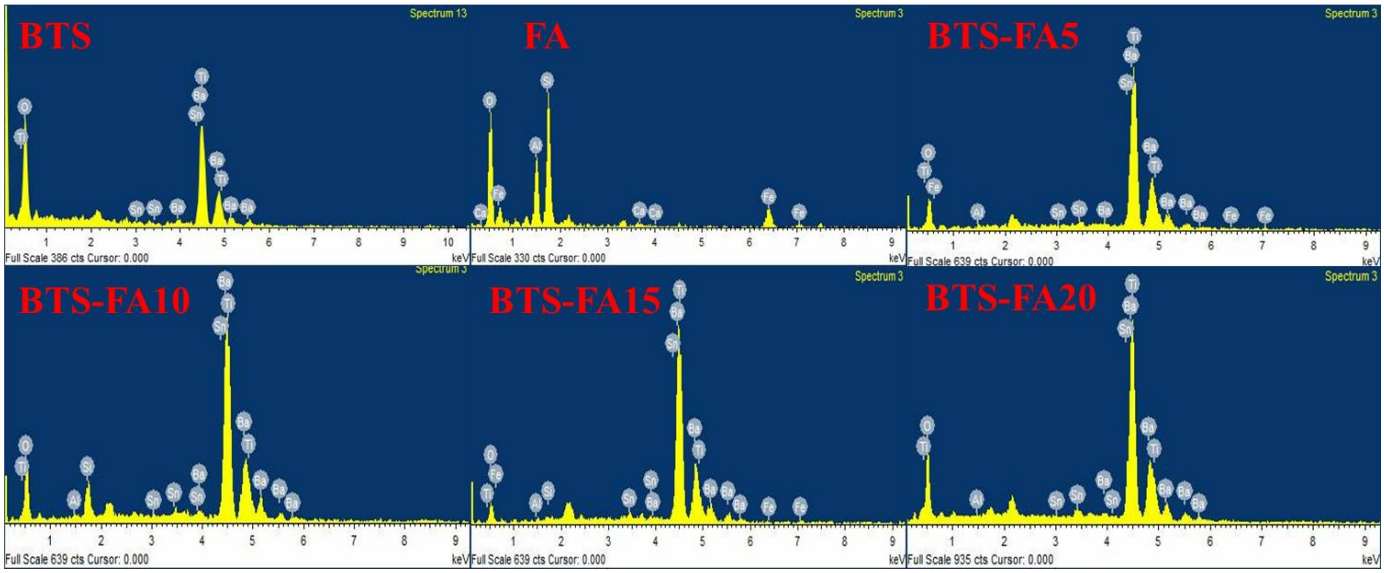


**Figure 7.7** Energy dispersive x-ray analysis (EDXA) of fractured surface of sintered samples

### 7.2.6 Dielectric Analysis

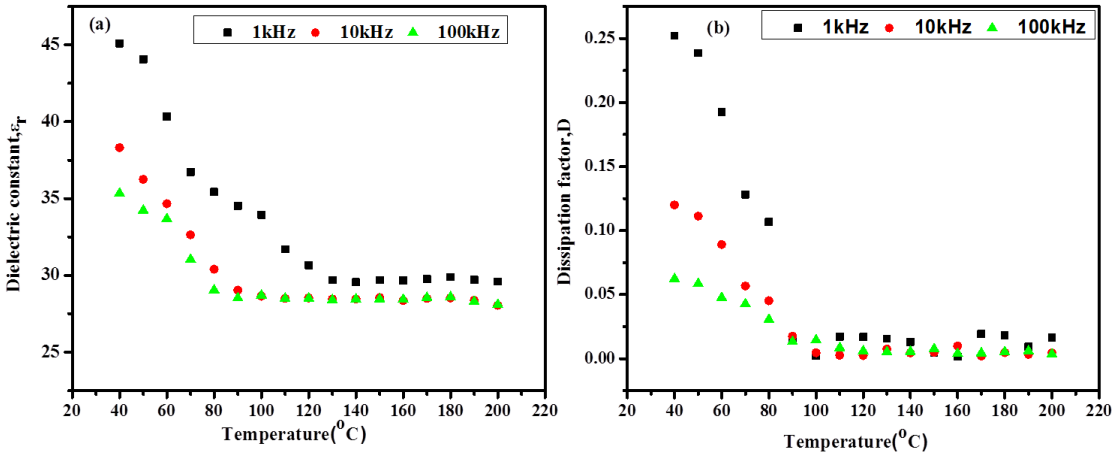


**Figure 7.8** Variation of (a) Dielectric constant (b) Dissipation factor with temperature of composite BTS-FA5

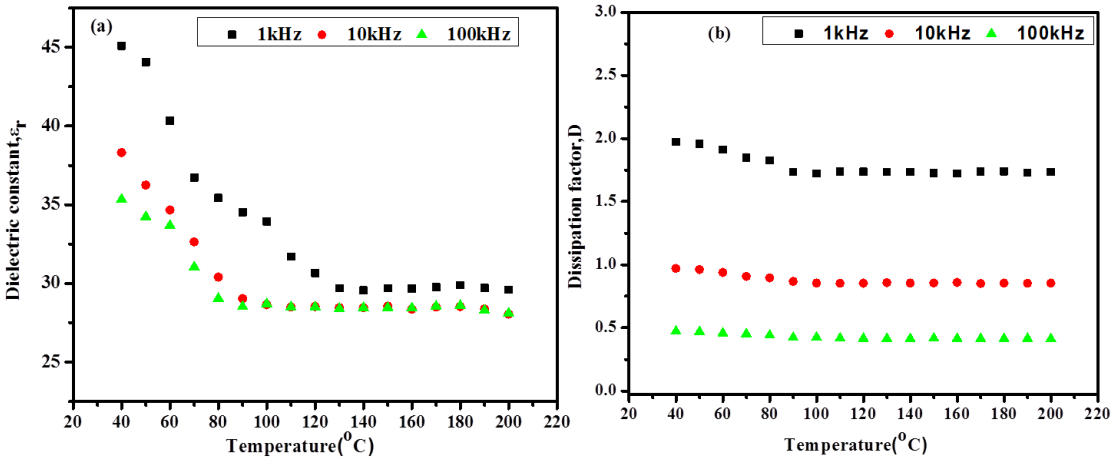


**Figure 7.9** Variation of (a) Dielectric constant (b) Dissipation factor with temperature of Composite BTS-FA20

Variation of dielectric constant and dissipation factor with temperature for two representative composite samples BTS-FA5 and BTS-FA20 at three different frequencies 1, 10 and 100 kHz are shown in Figure 7.8 and 7.9, respectively. On comparing value of dielectric constant of these composites with dielectric constant of sample BTS (shown in previous chapters) it is found that dielectric constant and dissipation factor of these composites BTS-FA5 and BTS-FA20 is lower than that of BTS. The decrease in the value of dielectric constant and dissipation factor may be due to insulating behavior of fly-ash [253]. Dielectric constant and dissipation factor remains almost constant with temperature within the investigated temperature range. Similar behavior was observed for other composites also. Experimental value of dielectric constant and dissipation factor of all the composites is given in Table 7.1. Theoretical value of dielectric constant of the composites calculated using mixture rule given by equation (7.1) is also sown in the same table for the comparison.

$$log\varepsilon_{eff} = \vartheta_1 log\varepsilon_{r1} + \vartheta_2 log\varepsilon_{r2} \quad (7.1)$$

Where $\vartheta_1$ and $\vartheta_2$ are the volume fraction of the phases BTS and FA while $\varepsilon_{r1}$ and $\varepsilon_{r2}$ are

dielectric constant of the phase BTS and FA respectively and $\varepsilon_{eff}$ is the dielectric constant for the composites. From Table 7.2 it is found that the value of dielectric constant calculated from Equation (7.1) higher than the experimental. This is may be due to decrease in dipole number, because in composite some of dipoles gets freeze and does not respond in presence of applied field, due to distribution of fly ash at the grains of BTS.

The dielectric constant and dissipation factor of composites BTS-FA were measured in the frequency range 40 Hz–2 MHz at few selected temperatures in the range of 30-200$^{o}$C. Variation of dielectric constant and dissipation factor with frequency for one of the representative composites BTS-FA5 was shown in Figure 7.10. Similar plot were observed for other composites also.

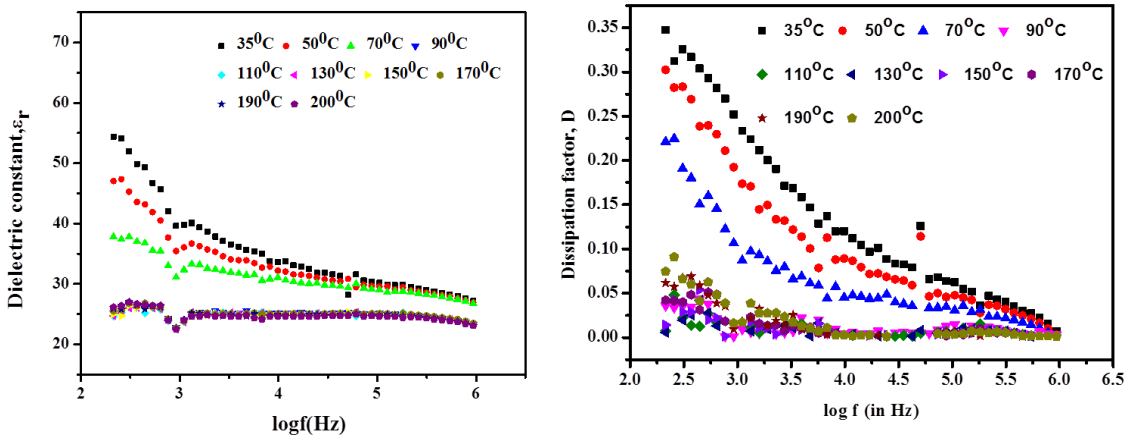


**Figure 7.10** Variation of Dielectric constant and Dissipation factor for composite BTS-FA5

Dielectric constants of samples decrease sharply up to 1 kHz frequency and thereafter attained constant value. At lower frequency dielectric constant has contribution of all types of polarization i.e. interfacial, orientation, ionic and electronic polarization. Below 1 kHz frequency mainly interfacial polarization contributes to the dielectric constant. Interfacial polarization in the composites is possible on account of presence of two different materials BTS and FA of

different conductivity value. At higher frequency, the internal individual dipoles contributing to the dielectric constant cannot move instantly, so as frequency of an applied voltage increases, the dipole response is limited and the dielectric constant decreases. Variation of dissipation factor with frequency is same as of dielectric constant. Similar results were obtained for other composites also.

### 7.2.7 Electrical Conductivity

Ac electrical conductivity, $\sigma_{ac}$ of two composites BTS-FA5 and BTS-FA20 were measured in the frequency range 40 Hz–2 MHz at few selected temperatures in the temperature range of 30-200$^{o}$C has also been carried to investigate conduction process. The plot of AC conductivity with respect to the logarithmic frequency has been shown in Figure 7.11.

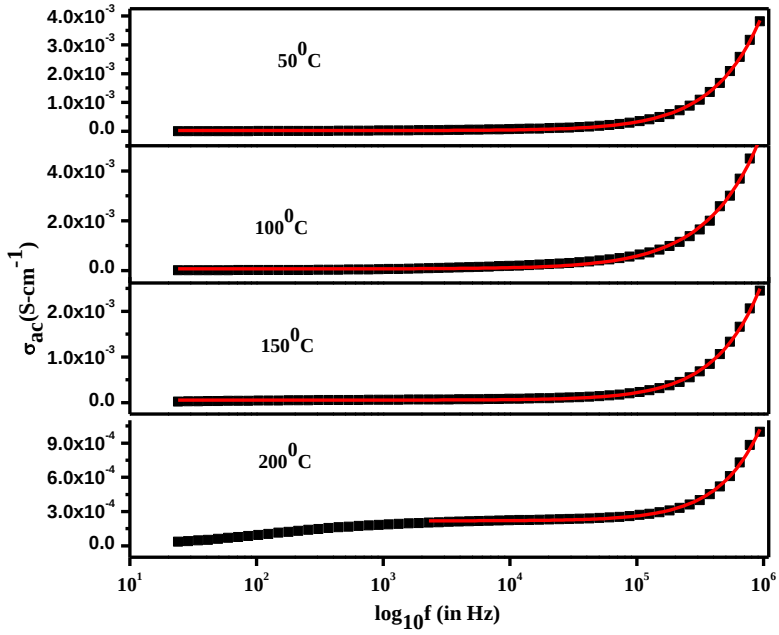


**Figure 7.11** Variation of ac conductivity with logarithmic of frequency for composite BTS-FA5, symbols represent experimental data and solid line shows fitted data.

The observed variation of $\sigma_{ac}$ with frequency follows Johnscher's universal power law already given by Equation (6.2) and rewritten below for the convenience;

$$\sigma(\omega) = \sigma_{dc} + A\,\omega^{n}, \qquad (7.2)$$

Where $\sigma_{dc}$ is d.c. (or frequency independent) conductivity, A is temperature dependent parameter and n lies in the range $0 < n < 1$. The Johnscher's equation (7.2) has been used to fit the experimental data points of the conductivity spectra of the samples presented in Figure 7.11. The symbols in these figures represent the experimental data, and solid lines represent the best fit to the data according to Johnscher's equation (7.2). The value of dc conductivity, $\sigma_{dc}$ was obtained from the fitting. The dc conductivity of semiconducting oxides is generally governed by Arrhenius type conduction process

$$\sigma_{dc} \propto \exp\left(-\frac{E_A}{k_B T}\right) \qquad (7.3)$$

Where $E_A$ is the activation energy for the dc conductivity. The variation of dc conductivity [$\log_{10}(\sigma_{dc})$] with reciprocal temperature (1000/T) for different composites BTS-FA5 and BTS20 is illustrated in Figure 7. 12. The solid lines represent the linear fit to the data points suggesting the Arrhenius like charge transport within the investigated temperature range.

The dc conductivity value of BTS5 and composites of BTS-FA were shown in Table 7.2. The dc conductivity abruptly decreases when contents of fly ash increases in samples. This confirms that fly ash having insulating properties. Low value of the activation energy indicates that in the temperature range 30-200$^{o}$C electronic conduction via hopping of charge carriers between $Sn^{2+}$ and $Sn^{4+}$ or $Fe^{2+}$ and $Fe^{3+}$ is taking place.

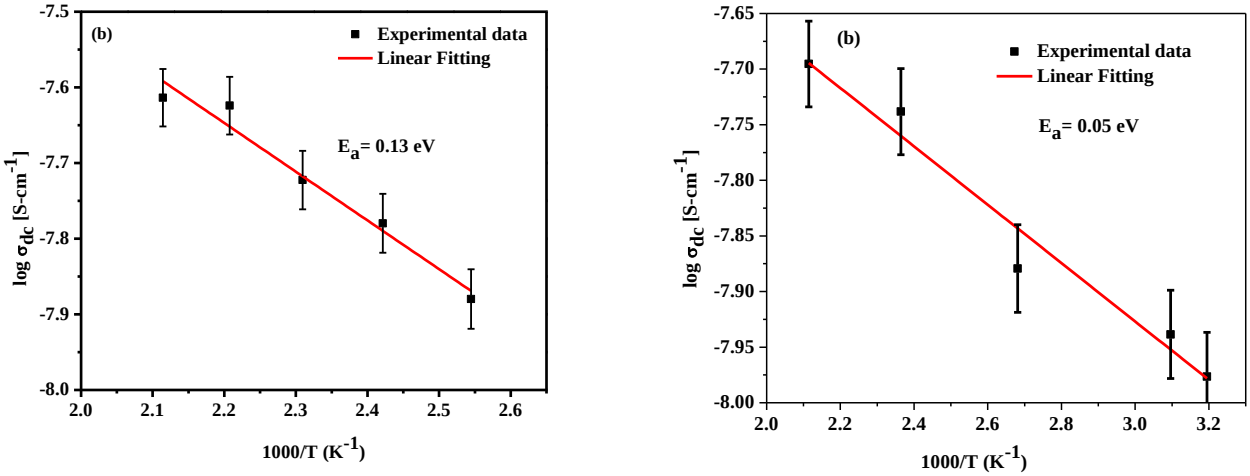


**Figure 7.12** Plots of $\log_{10}\sigma_{dc}$ versus 1000/T of (a) BTS-FA5 and (b) BTS-FA20 sintered samples

## 7.3 CONCLUSION

In this study we demonstrated that the fly-ash generally is the wastes which were used to enhance the properties of the barium titanate stannate. The analysis of composites was studied through TG-DSC and a preliminary study on the phase formation and determination of their crystal structure, the powder x-ray diffraction technique was adopted. The thermal analysis of the mixture of the composites shows the thermal stability of the samples with in the investigated range of temperature, while the XRD pattern shows no reaction among the two phases. The morphology of composite materials was studied by scanning electron microscopy (SEM) and analysis of grain size of composite (BTS-FA) carried out through "**Image J**" software which shows smaller grain size than barium titanate stannate (BTS). The dielectric constant and dissipation factor of composites was low as compared to BTS which reflects the insulating behavior of fly ash. The activation energy also decreases from 0.13 to 0.05 eV with increasing the fly ash content in barium titanate stannate samples, which reflects the locally migration of electron in between the respective sites of multivalent ion Sn/Ti and Fe. The lower value of dielectric constant and loss as well as insulating behavior of composites were may explore the application in field of high mechanical strength, high thermal and environmental stability, low

thermal expansion, low current leakage, low moisture absorption, corrosion resistant etc. Composites exhibit small value of dielectric constant and dissipation factor at higher frequency hence, they are more suitable for thermally stable capacitor fabrication as compared to BTS.